ELSEVIER

Contents lists available at ScienceDirect

## Atmospheric Environment

journal homepage: www.elsevier.com/locate/atmosenv





# High resolution source-resolved $PM_{2.5}$ spatial distribution and human exposure in a large urban area

Evangelia Siouti<sup>a</sup>, Ksakousti Skyllakou<sup>a</sup>, David Patoulias<sup>a</sup>, Eleni Athanasopoulou<sup>c</sup>, Nikolaos Mihalopoulos<sup>c</sup>, Jeroen Kuenen<sup>d</sup>, Spyros N. Pandis<sup>a,b,\*</sup>

- a Institute of Chemical Engineering Sciences (ICE-HT), Foundation for Research and Technology Hellas (FORTH), Patras, 26504, Greece
- <sup>b</sup> Department of Chemical Engineering, University of Patras, Patras, 26504, Greece
- Institute for Environmental Research and Sustainable Development, National Observatory of Athens (NOA), Athens, 11810, Greece
- <sup>d</sup> TNO, Department of Climate, Air and Sustainability, 3584 CB, Utrecht, the Netherlands

#### HIGHLIGHTS

- New source apportionment method for both local and regional fine PM.
- PM population exposure is influenced by local sources more than PM levels.
- Local biomass burning dominated both PM levels and exposure during winter.
- Long range transport was dominant during the winter.
- The modeling source apportionment results were consistent with measurements.

#### ABSTRACT

Chemical transport models often use moderate spatial resolution to simulate atmospheric pollution, thereby limiting the model's ability to represent variations in urban areas. Additionally, the contributions of individual sources of pollution transported to the urban areas of interest from elsewhere are rarely quantified. In this study, we developed an approach to simulate air quality, focusing on  $PM_{2.5}$  (particulate matter with a diameter lower than 2.5  $\mu$ m), and its local and regional sources at high spatial resolution of  $1 \times 1$  km<sup>2</sup>. The approach is applied in the largest city of Greece, Athens. The PMCAMx chemical transport model is employed in combination with the source apportionment algorithm, PSAT (Particle Source Apportionment Technology), to quantify the concentrations and sources of  $PM_{2.5}$ , organic aerosol (OA) and elemental carbon (EC) for a typical summer and winter month. A novel approach is developed, allowing the quantification of the contributions of sources not only inside the simulated urban area but also of the regional sources located outside. Model predictions were combined with population distribution data to provide estimations for human exposure not only to total  $PM_{2.5}$  concentrations but also to specific sources within the city. Residential biomass burning and transportation were found to be the dominant local sources of  $PM_{2.5}$  exposure. The higher resolution (1  $\times$  1 km<sup>2</sup>) offered a more detailed representation of  $PM_{2.5}$  spatial variability than a coarser one (36  $\times$  36 km<sup>2</sup>). This underscores the importance of capturing local sources in specific areas of the domain. The proposed approach can be used to provide estimates of human exposure to specific local and regional sources of primary and secondary  $PM_{2.5}$  in an urban area.

## 1. Introduction

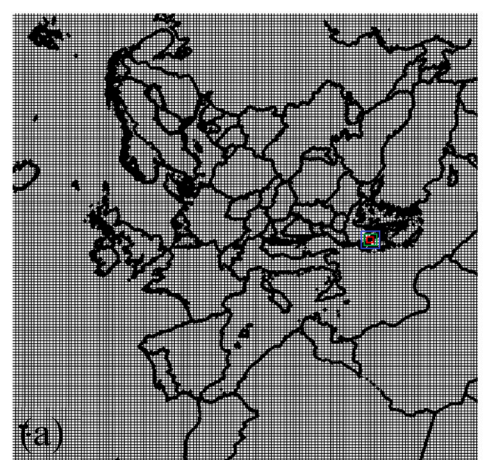
Fine particulate matter (PM) has serious effects on human health, as it causes heart diseases, respiratory disorders, lung cancer, or even death (Feng et al., 2016; Huang et al., 2017). Whereas coarse PM is more likely to deposit on the upper portion of the respiratory system, fine PM can enter the deeper regions of the lung causing increased damage (Deng et al., 2019; EPA, 2023). Even at low concentrations, PM<sub>2.5</sub> exposure can affect public health (Fann et al., 2012). In Europe, it is estimated that PM<sub>2.5</sub> is responsible for approximately 250 thousand premature deaths

annually (EEA, 2023).

The chemical composition of  $PM_{2.5}$  varies spatially, and often organics dominate the fine PM composition in Europe and the US (Zhang et al., 2007). Anthropogenic sources of PM include industry, transportation, residential heating, cooking, shipping, agriculture, etc.

Detailed field measurements are often used for  $PM_{2.5}$  source apportionment in one or more specific sites in a large urban area. For Athens, Theodosi et al. (2018), based on 848  $PM_{2.5}$  samples collected during a period of more than 2 years (12/2013-3/2016) at an urban background site, estimated the contribution of six sources, namely biomass burning

<sup>\*</sup> Corresponding author. Institute of Chemical Engineering Sciences (ICE-HT), Foundation for Research and Technology Hellas (FORTH), Patras, 26504, Greece. E-mail address: spyros@chemeng.upatras.gr (S.N. Pandis).



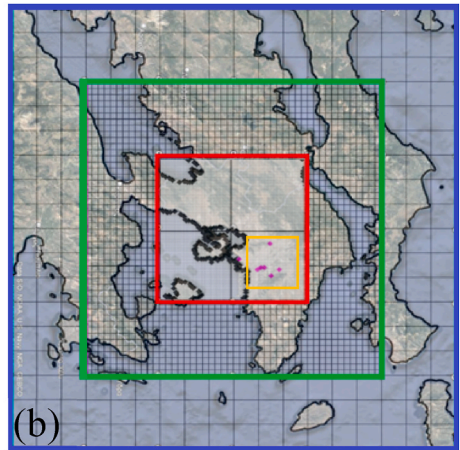


Fig. 1. (a) European modeling domain, (b) nested domains focusing on the  $1 \times 1$  km<sup>2</sup> modeling domain of Athens (red). Blue: 1st nested domain with  $12 \times 12$  km<sup>2</sup> spatial resolution, green: 2nd nested domain with  $3 \times 3$  km<sup>2</sup> spatial resolution and red the 3rd nested domain with  $1 \times 1$  km<sup>2</sup> spatial resolution (inner domain) and (c) inner domain with the locations of PM<sub>2.5</sub> sensors. Purple dots represent measurement sites. The orange box represents the urban center of Athens. (For interpretation of the references to colour in this figure legend, the reader is referred to the Web version of this article.)

(31 %), vehicular emissions (19 %), heavy oil combustion (7 %), regional secondary (21 %), marine aerosols (9 %), and dust particles (8 %). Similar results were also presented by Saraga et al. (2021) confirming that residential combustion was the predominant PM<sub>2.5</sub> source in an urban background site in Athens, contributed 38 % to PM<sub>2.5</sub> during 2017, followed by secondary particles (20 %), soil dust (12 %) and traffic (17%). In a traffic site, the traffic contribution increased to 27%, but residential combustion was still the major source. Pateraki et al. (2020) concluded that the predominant source of PM<sub>2.5</sub> during early spring and summer was biomass burning. Diapouli et al. (2017) found that biomass burning contributed 46 % to PM<sub>2.5</sub> in an urban site (at the south-eastern part of Athens) during 2011-2012, while sulfate was the most important contributor (55 %) to PM<sub>2.5</sub> in a suburban site ("Demokritos" campus) at the same period. In another urban background site (Zografou) in Athens, Grivas et al. (2018) found that almost half of PM<sub>2.5</sub> was due to regional pollution during 2011-2012. Traffic contributed 24 % to PM<sub>2.5</sub>, biomass burning 9 %, mineral dust 7 %, oil combustion 4 %, and sea-salt 2 %.

PM<sub>2.5</sub> source apportionment modeling studies often employ low spatial resolution due to their high computational cost and the lack of suitable high-resolution emission inventories. For example, Thunis et al. (2018) used the SHERPA (Screening for High Emission Reduction Potentials for Air quality) tool, which is a simplified version of a chemical transport model, at the spatial resolution of 7 km<sup>2</sup>. This study estimated that industry was the major source of PM<sub>2.5</sub> in Athens during 2009. However, there have been significant changes in emissions in Athens during the last decade. In addition, higher spatial resolution allows for a more accurate representation of the variability in source contributions across the city, leading to a better understanding of pollutant distribution and spatial patterns (Garcia Rivera et al., 2022). Coelho et al. (2022) using the Comprehensive Air Quality Model (CAMx) and PSAT, estimated that long-range transport was the dominant contributor to PM concentration levels in both summer and winter in six major European cities. Pepe et al. (2019) also using CAMx/PSAT showed the importance of regional sources for PM2.5 in Milan during the year. While these studies provided valuable insights about the relative importance of the various local sources in major urban areas, they provided little information about the type of sources contributing to long-range transported fine PM<sub>2.5</sub>. At the same time, challenges in estimating the source contributions to secondary PM<sub>2.5</sub> (especially OA) remain. This secondary fraction can dominate the PM<sub>2.5</sub> levels during most of the year.

In this study, we combine the PMCAMx model and the PSAT source apportionment algorithm to produce source-apportioned PM<sub>2.5</sub> predictions at a high spatial resolution of 1  $\times$  1 km $^2$  for a European city

(Athens) for 2019 during a summer and a winter month. The model results, in combination with the population distribution in the city, are then used to estimate human exposure not only to total  $PM_{2.5}$  concentration but also to local and regional sources. The novelty of this work lies in the further separation and analysis of the contribution of individual sources located outside the urban domain.

#### 2. Model description and application

#### 2.1. The PMCAMx model

The three-dimensional chemical transport model PMCAMx (Particulate Matter Comprehensive Air quality Model with extensions) (Fountoukis et al., 2011) is utilized in this study to simulate the pollutant concentrations in a European city, Athens (Greece). PMCAMx solves the continuity equation for each pollutant at each time-step. The injection of emissions from all sources is the first simulated process in each step. Following this, PMCAMx simulates vertical and horizontal advection, chemistry, vertical and horizontal dispersion, and dry/wet removal. Gas-phase chemistry is simulated using the SAPRC mechanism (Carter, 2000), which includes 217 reactions and 114 species (16 radicals, 76 gases). For aerosol chemistry, the bulk equilibrium approach is utilized for the partitioning of inorganic and secondary organic compounds between the gas and particle phases (Capaldo et al., 2000). The Variable Size Resolution Model developed by Fahey and Pandis (2001) is applied for the simulation of aqueous-phase chemistry.

For organic aerosol, the 1-D Volatility Basis Set (VBS) approach (Donahue et al., 2006) is used for primary and secondary OA, treating both as chemically reactive and semi-volatile components. The organic components were separated into logarithmically spaced volatility bins based on their effective saturation concentration at 298 K. The parameterizations used were those of Tsimpidi et al. (2010).

Wet deposition is modeled applying a scavenging model for aerosol and gases (Seinfeld and Pandis, 2006), while the methodology of Wesely (2007) and Slinn and Slinn (1980) is used for dry deposition simulation. The approach of Tambour and Seinfeld (1980) is employed to model aerosol particle coagulation.

## 2.2. Model application

In this first application of the proposed methodology, we focused on air pollution in Athens, Greece. PMCAMx was applied all over Europe focusing on the city of interest using three nested grids with increasing spatial resolution. The outer domain was the European domain (low-

resolution grid), which extended over an area of  $5400 \times 5832 \text{ km}^2$  with a  $36 \times 36 \text{ km}^2$  horizontal spatial resolution (Fig. 1). The inner domain covered a region of  $72 \times 72 \text{ km}^2$  for the city using  $1 \times 1 \text{ km}^2$  spatial resolution. Also, there were two other intermediate grids with  $12 \times 12$  and  $3 \times 3 \text{ km}^2$  resolutions that were centered on the city. There were 14 layers in the vertical for each of the modeling domains.

#### 2.2.1. Meteorology

The study periods were a typical winter (January) and a summer (July) month during 2019. The meteorological data were produced by the Weather Research and Forecasting (WRF) mesoscale numerical prediction model (Skamarock et al., 2019) using the same grids as PMCAMx. The WRF output data were used directly for the  $36 \times 36 \text{ km}^2$  European domain and the inner  $1 \times 1 \text{ km}^2$  domain. Interpolated meteorological data about the zooming approach were used for the other two nested domains at  $12 \times 12$  and  $3 \times 3 \text{ km}^2$ . Additional details can be found in Siouti et al. (2022, 2024).

#### 2.2.2. Emissions

The anthropogenic emissions were based on the CAMS-REG-v4 inventory developed by the Netherlands Organization of Applied Scientific Research (TNO) at a  $0.05^{\circ} \times 0.1^{\circ}$  grid resolution (Kuenen et al., 2022). There are twelve source sectors including industry, public power, road transport, non-road transport, agriculture, shipping, aviation, domestic processes, fugitives, solvents, waste processes and agricultural waste burning. The emission inventory includes the main atmospheric pollutants (SO<sub>2</sub>, NO<sub>x</sub>, non-methane volatile organic compounds, NH<sub>3</sub>, CO, PM<sub>10</sub> and PM<sub>2.5</sub>). PM components include elemental carbon, organic carbon, sulfate, sodium and other minerals. Non-methane volatile organic compound emissions have been split into 23 groups. The emissions for the European domain were prepared initially at  $36 \times 36$  km² spatial resolution following the corresponding PMCAMx grid. Point emissions from industry, heat plants, airports and waste treatment plants were placed in the corresponding grid cell.

For the estimation of high-resolution emissions for the inner domain, we disaggregated spatially the 36  $\times$  36 km $^2$  TNO emission inventory using the UrbEm method and tool (Ramacher et al., 2021). UrbEm combined the CAMS emissions dataset with selected high resolution spatial proxies per source category. The output of the tool is an emission inventory for any city or region in Europe, at the spatial resolution of interest. For the current application, the UrbEm results were normalized and were used for the distribution of the 36  $\times$  36 km $^2$  TNO emissions to  $1\times1~\mathrm{km}^2$  keeping the totals the same.

Biomass burning OA (bbOA) emissions for the high-resolution domain were estimated in this study, based on Siouti et al. (2024) at approximately 18 tn  $\rm d^{-1}$ . These emissions are associated with biomass burning in fireplaces and woodstoves, which has become a major residential heating method in Greece after the financial crisis in the 2010s. These emissions are underestimated in the TNO emissions inventory. Spatial, temporal and volatility distribution of wood combustion emissions for the urban area of Athens are presented in Fig. S1.

## 2.3. The PSAT source apportionment algorithm

The PSAT algorithm was applied to calculate the source contributions to  $PM_{2.5}$ , OA and EC for both primary and secondary material (Skyllakou et al., 2014; Skyllakou et al., 2021; Skyllakou et al., 2017; Wagstrom et al., 2008, 2011a, 2011b). PSAT operates in parallel with PMCAMx and is highly computationally efficient. In this application, PSAT tracks the following source categories of both primary and secondary PM separately: agriculture, shipping, aviation, waste burning, heat plants, industry, biomass burning, combustion, solvents and fugitives, exhaust road transport, non-exhaust road transport, non-road transport, initial and boundary conditions. The "biomass burning" source corresponds to bbOA, as described in Section 2.2.2, and is specifically associated with biomass burning in fireplaces and wood stoves

for residential heating. In contrast, the "combustion" source refers to domestic combustion primarily for cooking and residential heating with fuels (gas, liquid and solids) other wood.

PSAT has been designed to determine source contributions within a single modeling domain with a fixed spatial resolution. PSAT was extended in this work to provide source contributions using multiple grids and moving from the regional to the urban scale with increasing spatial resolution. As a result, in our approach, we estimate separately the contributions of these local sources and the corresponding sources outside the domain.

The extended algorithm uses the following steps: (a) PSAT is used at the  $36\times36~\mathrm{km}^2$  modeling domain over Europe, (b) for each  $36\times36~\mathrm{km}^2$  grid cell, the average concentration of each pollutant due to each source is calculated, (c) PSAT is used at the  $1\times1~\mathrm{km}^2$  modeling domain over the city of interest, (d) for each  $1\times1~\mathrm{km}^2$  grid cell, the average concentration of species coming from each local source is calculated, (e) the transported concentrations in the  $1\times1~\mathrm{km}^2$  domain for each source are calculated by subtracting the local concentrations from step (d) from the total  $36\times36~\mathrm{km}^2$  average concentrations obtained in step (b), and (f) the results of step (d) and step (e) are synthesized to provide the contribution of all sources separated into local and transported contributions for each pollutant of interest.

#### 2.4. Quality assessment

#### 2.4.1. Measurements

For the evaluation of PM<sub>2.5</sub> predictions we used measurements from seven sites equipped with low-cost PM<sub>2.5</sub> sensors located in the urban core of Athens (Thissio, Keratsini, Gyzi, Vathis Square, Chalandri, Ano Liosia and Papagou). The locations of the low-cost sensors are shown in Fig. 1. Kosmopoulos et al. (2020) assessed the accuracy of these sensors for Greece and recommended the following correction for PM<sub>2.5</sub>: PM<sub>2.5</sub> = 0.42 PAir<sub>2.5</sub> + 0.26 ( $\mu$ g m<sup>-3</sup>), where PM<sub>2.5</sub> is the corrected concentration and PAir<sub>2.5</sub> is the measured value. This correction was applied to all the data that will be used in the rest of the study. The urban center of Athens that we will focus on is a 20 × 20 km<sup>2</sup> part of the inner modeling domain (Fig. 1).

Aerosol chemical speciation monitor (ACSM) (Aerodyne Inc., USA) measurements from the National Observatory of Athens (NOA) at Thissio, in the center of Athens, were also used. The measurement resolution was 30 min. Also, an aethalometer that was operated by NOA was used to measure black carbon (BC) concentrations. More details about ACSM and BC measurements at the Thissio site can be found at Stavroulas et al. (2019).

## 2.4.2. Metrics

The mean bias (MB), fractional bias (FBIAS), mean error (ME) and fractional error (FERROR) were used to evaluate the model performance of  $PM_{2.5}$ , OA and EC. The evaluation metrics are given by the following equations:

$$MB = \frac{1}{N} \sum_{i=1}^{n} (P_i - O_i)$$
  $ME = \frac{1}{N} \sum_{i=1}^{n} |P_i - O_i|$ 

$$FBIAS = \frac{2}{N} \sum_{i=1}^{n} \frac{(P_i - O_i)}{(P_i + O_i)} \qquad FERROR = \frac{2}{N} \sum_{i=1}^{n} \frac{|P_i - O_i|}{(P_i + O_i)}$$
(1)

where N is the total number of measurements,  $P_i$  is the predicted concentration and  $O_i$  is the corresponding observed concentration of the evaluated species.

Based on Morris et al. (2005) PM<sub>2.5</sub> model performance for daily average values is considered excellent for FBIAS  $\leq \pm 15$ % and FERROR  $\leq \pm 35$ %, good for FBIAS  $\leq \pm 30$ % and FERROR  $\leq \pm 50$ %, average for FBIAS  $\leq \pm 60$ % and FERROR  $\leq \pm 75$ %, while there are fundamental problems in the modeling system for higher FBIAS and FERROR.

Table 1 Daily average  $PM_{2.5}$ , OA and EC predictions and measurements for July and January 2019 for different sites in Athens.

Site	Туре	July 2019		January 2019		
		Observed (μg m <sup>-3</sup> )	Predicted (μg m <sup>-3</sup> )	Observed (μg m <sup>-3</sup> )	Predicted (μg m <sup>-3</sup> )	
		PM <sub>2.5</sub>				
Thissio	Urban-	8.2	9.2	12	13.8	
	background					
Keratsini	Urban-	7.5	7.7	_	_	
	background					
Gyzi	Urban-	7.5	8.5	-	-	
	background					
Vathis	Urban-	8.5	8.7	-	-	
Square	background					
Chalandri	Suburban-	8.4	8.2	-	_	
	background					
Ano	Urban-	_	-	15.4	12.4	
Liosia	background					
Papagou	Suburban-	7.2	8.4	7.4	8.5	
	background					
		OA	_			
Thissio		4.5	3	11	9.5	
mi · ·		EC	0.60	0.0	1.0	
Thissio		0.6	0.68	2.3	1.6	

#### 2.5. Population exposure

The population distribution for the city of Athens was determined using population data from the European Union. The analysis utilized the most recent database, the Eurostat census grid 2021 (https://ec.europa.eu/eurostat/web/gisco/geodata/grids). This dataset, which pertains to 2021, is provided at a high spatial resolution of  $1\times 1~\text{km}^2$ . Athens has a total population of 3.3 million residents within the inner simulation area. The number of inhabitants in each  $1\times 1~\text{km}^2$  grid cell is multiplied by the average predicted PM2.5 concentration for that cell, producing population exposure maps with a  $1\times 1~\text{km}^2$  spatial resolution. This exposure metric reflects the overall damage caused to the health of the population of each  $1\times 1~\text{km}^2$  area by total PM2.5 as well as its individual sources and components.

#### 3. Results

#### 3.1. Model evaluation

In summer, PMCAMx predicted the highest average  $PM_{2.5}$  concentration of 9.2  $\mu g\ m^{-3}$  in Thissio (Table 1). The differences between measured and predicted values were lower than 1  $\mu g\ m^{-3}$  in Thissio, Keratsini, Gyzi, Vathis Square and Chalandri. Mean bias ranged from -0.24 to  $1.2\,\mu g\ m^{-3}$  and mean error from 2.4 to  $3.5\,\mu g\ m^{-3}$  in all studied sites

Model performance was excellent according to the criteria of Morris et al. (2005) for the urban sites of Thissio, Keratsini, Gyzi and Vathis Square with FBIAS  $\leq$  15 % and FERROR < 35 %, whereas it was good for Chalandri and Papagou with FBIAS  $\leq$  30 % and FERROR < 50 % (Table 2). Overall, the model's performance in reproducing PM<sub>2.5</sub> concentrations was good across all sites, with overall FBIAS equal to zero and FERROR of 45 %. For OA, model performance was average (FBIAS = -50 % and FERROR = 68 %) in Thissio, while it was considered excellent for EC with FBIAS equal to 9 % and FERROR equal to 24 %.

During winter, the model predicted the highest  $PM_{2.5}$  levels in Thissio of  $13.8~\mu g\ m^{-3}$ , while measurements indicated the highest  $PM_{2.5}$  concentration in Ano Liosia at  $15.4~\mu g\ m^{-3}$ . High mean error values for Thissio and Ano Liosia were attributed to uncertainties in residential biomass burning emissions during that period. At the suburban site of Papagou, measurements showed the lowest  $PM_{2.5}$  levels, consistent with the predictions, with average concentrations differing by less than  $1~\mu g\ m^{-3}$ . At this site, observed  $PM_{2.5}$  concentrations were approximately half of those measured in the city center.

The performance of PMCAMx for PM $_{2.5}$  during winter was good for all sites individually. Looking at all PM $_{2.5}$  data at all sites together, performance was good, with FBIAS equal to 38 % and FERROR equal to 15 %. For total OA, in the city center, the model's performance was average, with an FBIAS of -20 % and an FERROR of 57 %. The model performed well in predicting EC in Thissio, with a mean bias of -0.67  $\mu g$  m $^{-3}$  and a mean error of 0.87  $\mu g$  m $^{-3}$  and a good model performance.

#### 3.2. Predicted source contributions in summer

During summertime, long-range transport (LRT) was the predominant source of PM<sub>2.5</sub> in the  $1 \times 1$  km<sup>2</sup> modeling domain, with an average contribution of 90 % (Fig. 2a) and an average concentration of 6 μg m<sup>-3</sup> (Fig. 3) in agreement with Dimitriou et al. (2023). A significant fraction (28 %) of transported PM<sub>2.5</sub> was due to wildfires, 16 % from industry, 12 % from biogenic and marine sources, 8 % from agriculture, 7 % from shipping, 4 % from road transport, 3.5 % from combustion 2.5 % from fugitives and solvents and the rest from outside Europe. The major local sources of  $PM_{2.5}$  were shipping (3 % of total  $PM_{2.5}$ ), industry (2.5 %) and transportation (1.6 %). Higher levels of  $PM_{2.5}$  were predicted in the northeast of the city (Fig. 4), with a total average PM2.5 concentration for the 1  $\times$  1 km<sup>2</sup> domain equal to 6.6  $\mu$ g m<sup>-3</sup>. In the urban core, long-range transport was also the primary source of PM2.5 but with a lower average contribution of 81 % than the whole inner domain (Fig. 2b). In this area, 37 % of transported PM<sub>2.5</sub> was attributed to wildfires. The major local sources in the city center were industry, road-transport and fugitives and solvents, each contributing 5 % to PM<sub>2.5</sub> on average. PM<sub>2.5</sub> concentrations of 2.5  $\mu$ g m<sup>-3</sup> related to shipping were predicted around the Port of Piraeus, which is the biggest port in the country (Fig. 3). In the urban center, PM<sub>2.5</sub> levels ranged from 8 to 9.6  $\mu$ g m<sup>-3</sup>, with an average value of 8.5  $\mu$ g m<sup>-3</sup> (Fig. 4).

Table 2
Metrics for daily average PM<sub>2.5</sub>, OA and EC predictions and measurements for July and January 2019 for different sites in Athens.

Site	July 2019				January 2019			
	MB (μg m <sup>-3</sup> )	ME ( $\mu g m^{-3}$ )	FBIAS (%)	FERROR (%)	MB (μg m <sup>-3</sup> )	ME ( $\mu g m^{-3}$ )	FBIAS (%)	FERROR (%)
	PM <sub>2.5</sub>							
Thissio	1	2.6	10	29	1.6	5.4	7	42
Keratsini	0.24	2.4	0	34	_	_	_	_
Gyzi	1	3	5	35	_	_	_	_
Vathis Sq.	0.26	3	-4	35	_	_	_	_
Chalandri	-0.24	3.5	-13	40	_	_	_	_
Ano Liosia	_	_	_	_	-3	6	-18	45
Papagou	1.24	3.4	2	39	1.15	2.9	15	38
	Total OA							
Thissio	-1.6	2.5	-50	68	-1.4	6.5	-20	57
	EC							
Thissio	0.09	0.16	9	24	-0.67	0.87	-25	41

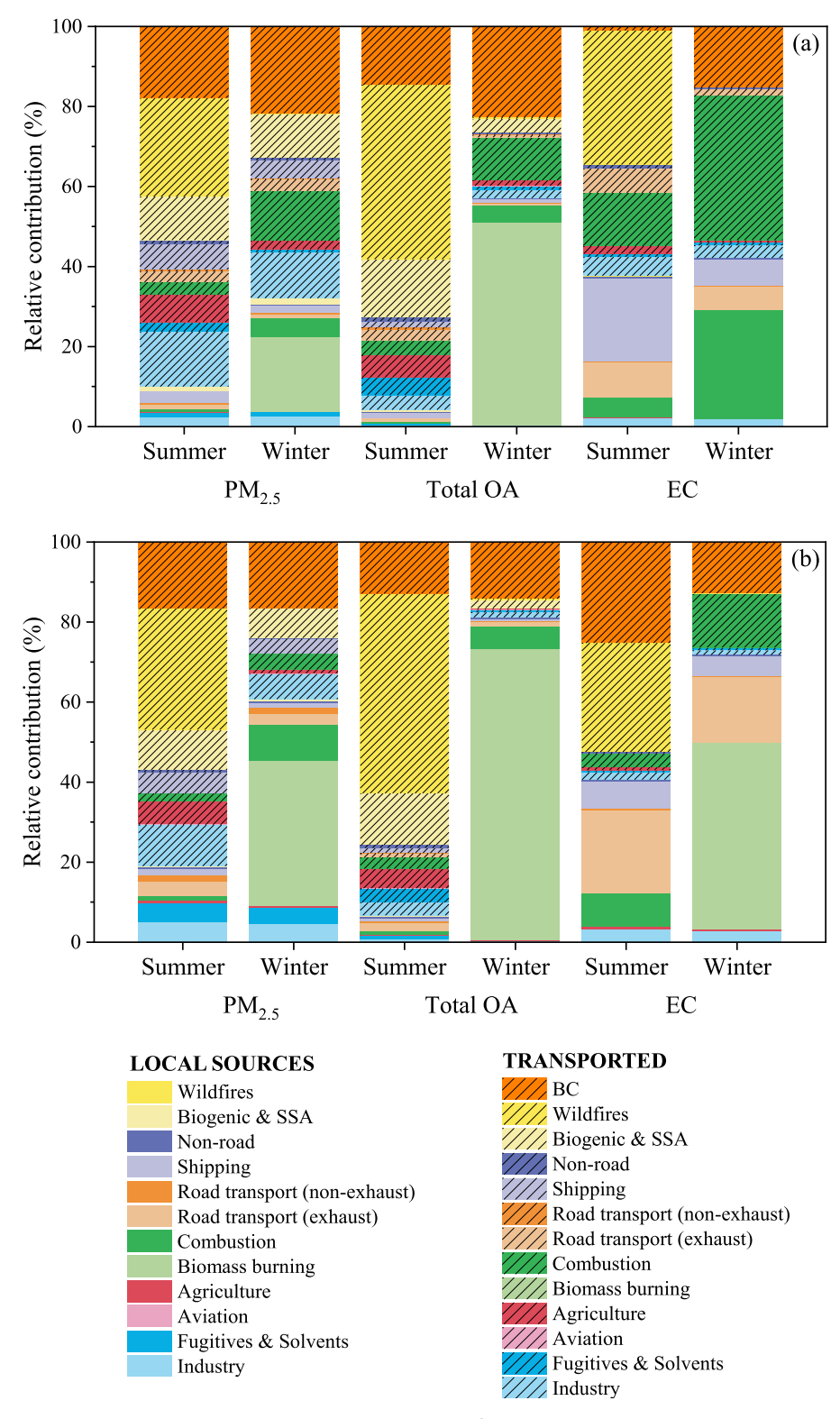


Fig. 2. Average predicted source contributions for PM<sub>2.5</sub>, OA and EC for (a) the  $1\times1$  km<sup>2</sup> modeling domain and (b) the urban center during July and January 2019.

On average, 96 % of total OA in the  $1\times1$  km² modeling domain originated from long-range transport (Fig. 2a). A substantial fraction (46 %) of this transported OA was due to wildfires, followed by biogenic and marine sources (15 %). The predominant local OA source was shipping (1.3 %). In the urban center, the most important local source was road transport (2.5 %), while the remaining local sources contributed less than 1 % each (Fig. 2b). Transported OA had higher levels in the northeast of the city, up to 4.5  $\mu$ g m³, while in the rest of the 1  $\times$  1

km² modeling domain, OA exhibited little spatial variation (Fig. S2). The average OA concentration related to long-range transport was 3.2  $\mu g \ m^{-3}$  in the urban core. Total predicted OA had low spatial variability, with an average concentration of 2.6  $\mu g \ m^{-3}$  in the inner domain (Fig. 4). Primary OA contributed 11 % to total OA, while secondary OA accounted for the rest. For the urban center, the average total OA was 3.4  $\mu g \ m^{-3}$ , with values ranging from 3.2 to 4.5  $\mu g \ m^{-3}$  (Fig. 4). In this area, primary OA contributed 22 % to total OA.

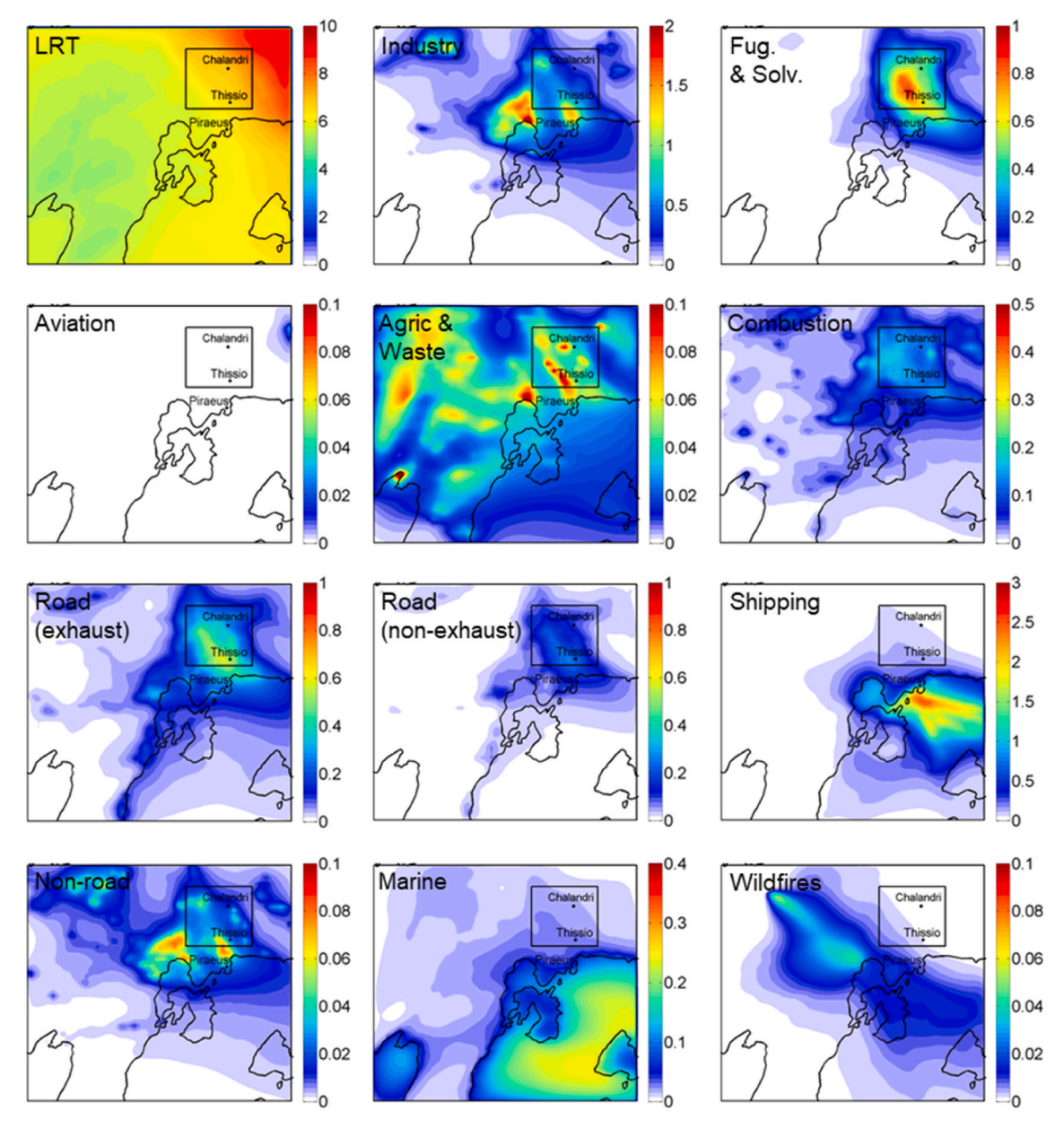


Fig. 3. Average predicted concentrations of  $PM_{2.5}$  from various sources in  $\mu g \ m^{-3}$  during July 2019 in Athens. The square indicates the center of Athens. Different scales are used.

Long-range transport was the dominant source of EC in the  $1\times1~km^2$  modeling domain, with an average contribution of 62 % (Fig. 2a). A significant fraction (55 %) of transported EC was attributed to wildfires, 22 % to combustion, 10 % to road-transport and 7 % to industrial sources. The most important local sources were shipping (21 %), traffic (9 %) and combustion (5 %) (Fig. S3). In the urban core, local traffic was the major local source, accounting for 21 % of EC (Fig. 2b). The highest EC concentrations were predicted near the port of Piraeus, while the total predicted EC had an average concentration of 0.4  $\mu$ g m<sup>-3</sup> within the inner modeling domain (Fig. 4).

#### 3.3. Predicted source contributions in winter

During wintertime, long-range transport accounted for 68 % to PM<sub>2.5</sub> in the  $1 \times 1 \text{ km}^2$  modeling domain with an average concentration of 3.7  $\mu g \text{ m}^{-3}$  (Fig. 2a). Combustion (18 %), industry (17 %) and biogenic and marine sources (16 %) outside the inner domain were major sources of transported PM<sub>2.5</sub>. Local residential biomass burning contributed 19 %

of the PM<sub>2.5</sub>, combustion 5 % and industry 3 %. In the urban center, residential biomass burning was the primary local source of PM<sub>2.5</sub>, contributing 37 % on average, followed by combustion (9 %), industry (5 %), fugitives and solvents (4 %), road transport (4 %) and shipping (1 %) (Fig. 2b). The other 40 % of PM<sub>2.5</sub> was transported from outside the inner domain. PM<sub>2.5</sub> from residential biomass burning had an average concentration of 1  $\mu g$  m $^{-3}$  in the inner modeling domain and 3.7  $\mu g$  m $^{-3}$  in the urban core (Fig. 5). Residential biomass burning PM<sub>2.5</sub> reached up to 8  $\mu g$  m $^{-3}$  at the north of the urban core, indicating the substantial impact of biomass burning on pollution levels in certain areas of the city. For total PM<sub>2.5</sub>, an average concentration of 10  $\mu g$  m $^{-3}$  was predicted for the urban core, nearly double the whole inner domain. The highest PM<sub>2.5</sub> concentration, 16  $\mu g$  m $^{-3}$ , was predicted in the center of the city, highlighting again the significance of local sources during the cold period.

Local residential biomass burning was the major OA source, contributing 51 % on average in the inner domain (Fig. 2a). Transported OA contributed 43 % of the total OA in the  $1 \times 1$  km<sup>2</sup> modeling domain.

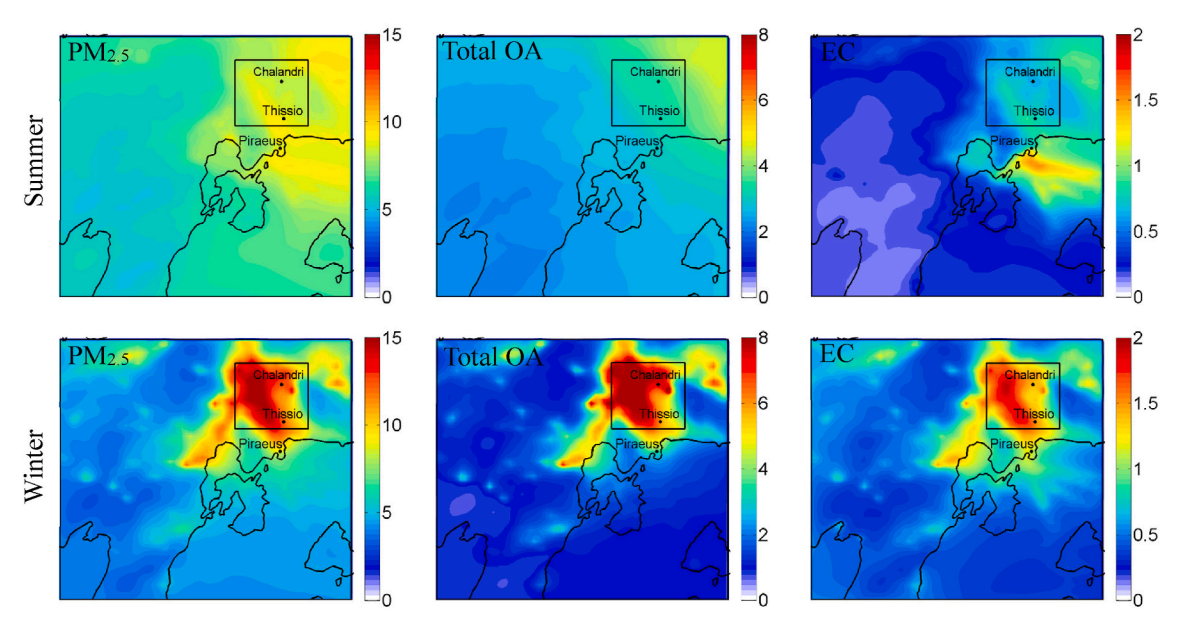


Fig. 4. Average predicted ground concentrations ( $\mu g \ m^{-3}$ ) of PM<sub>2.5</sub>, total OA and EC during July and January 2019 for the inner domain. The square indicates the center of Athens. Different scales are used.

In the city center, residential biomass burning was the dominant source, accounting for 73 % of total OA. Significant spatial variability in OA concentrations was predicted in the urban core due to residential biomass burning (Fig. S4). The total average OA concentration in the Athens center was 3.7 μg m<sup>-3</sup>, compared to an average of 1 μg m<sup>-3</sup> across the  $1 \times 1 \text{ km}^2$  modeling domain (Fig. 4). The highest OA concentration in the urban core was around 8 µg m<sup>-3</sup>. Significant spatial variations were predicted in the urban core also due to residential combustion and traffic (Fig. 5). Additionally, significant OA variation was predicted around the Port of Piraeus, primarily due to shipping activities. The average total OA concentration for the inner domain was  $2 \mu g m^{-3}$ , with primary OA contributing according to PMCAMx 70 % of the total OA during this period. In the urban core, OA concentrations ranged from 2 to 9  $\mu g$  m<sup>-3</sup>, with an average of 5  $\mu g$  m<sup>-3</sup>. PMCAMx indicated that primary OA dominated in the city center, contributing 88 % to the OA.

Long-range transport accounted for 58 % of EC in the  $1\times 1~{\rm km}^2$  modeling domain. A significant fraction of transported EC was due to wood combustion (63 %). In the city core, local combustion from domestic processes (mainly for heating) was predicted to be the dominant source, with an average contribution of 46 %. Spatial distributions of EC from combustion and road transport were highly variable in the urban core. The average total predicted concentration of EC for the inner modeling domain was  $0.6~{\rm \mu g~m}^{-3}$ , while for the urban center it was  $1.2~{\rm \mu g~m}^{-3}$ . Around the Port of Piraeus, the average predicted EC concentration was  $1~{\rm \mu g~m}^{-3}$  mainly due to shipping (Fig. S5).

## 3.4. Average diurnal variability of $PM_{2.5}$

Fig. 6 depicts the average measured and predicted diurnal profiles of PM<sub>2.5</sub> during summer. In all studied sites, both the measured and predicted diurnal profiles were relatively flat, supporting the conclusion that long-range transport was the predominant source of PM<sub>2.5</sub> during this period. In the urban site of Thissio, PM<sub>2.5</sub> measurements indicated a small increase of 2  $\mu g$  m $^{-3}$  during the night, consistent with the predictions. For the rest of the day, the measured and predicted average PM<sub>2.5</sub> concentrations were similar, around 7  $\mu g$  m $^{-3}$ . In the other urban sites of Keratsini, Gyzi and Vathis Square, the model reproduced the nighttime peak, which was slightly overestimated in Gyzi (2  $\mu g$  m $^{-3}$ ). Based on PSAT, the nighttime peak was mostly due to local transportation. In the suburban site of Chalandri, the measured PM<sub>2.5</sub> peak

during the afternoon was underestimated by the model, probably due to underestimation of local transportation emissions. On the other hand, in Papagou, the model reproduced the afternoon peak at  $10~\mu g~m^{-3}$  but with a 1-h difference. Predicted  $PM_{2.5}$  concentrations in this location increased between 10:00 and 16:00 LT due to a combination of vertical mixing of wildfire smoke and the formation of secondary aerosols through photochemical reactions. The overestimation of the  $PM_{2.5}$  during this period could be due to a combination of errors in the simulation of the local meteorology, regional source emissions, and the simulated secondary aerosol production.

During wintertime, PMCAMx reproduced the overall measured diurnal profiles across all sites (Fig. 7). In Thissio, measured PM2.5 peaked at 22:00 LT, reaching 24  $\mu g$  m<sup>-3</sup>, while the predicted PM<sub>2.5</sub> peaked at the same time at 33  $\mu g$  m<sup>-3</sup>. In the morning, at 9:00 LT, the model predicted a peak of 12  $\mu g$  m<sup>-3</sup>, which was 3  $\mu g$  m<sup>-3</sup> higher than the measured one. During the hour of maximum PM<sub>2,5</sub> levels, the model predicted that 65 % of the PM<sub>2.5</sub> originated from residential biomass burning. At Ano Liosia, the measured and predicted nighttime peaks differed by 1 h. The measured peak of 30  $\mu g$  m<sup>-3</sup> was observed at 22:00 LT, while the predicted peak of 34  $\mu g$  m<sup>-3</sup> occurred at 21:00 LT. The measured morning peak was underestimated by the model, and there was also a 1-h difference. This underestimation is likely related to underestimated transportation and biomass burning emissions during these hours. In Papagou, measurements peaked at 14  $\mu g m^{-3}$  at 22:00 LT, while the predicted value peaked at 20  $\mu g$  m<sup>-3</sup> at the same hour. During the morning, PMCAMx overpredicted the peak by an average of  $2 \mu g m^{-3}$ . The model consistently overestimated the nighttime peak across all sites by 20-40 %, mainly due to uncertainties in the residential biomass burning contribution, particularly in its spatial and temporal distribution. It should be noted that the measurements are from low-cost PM<sub>2.5</sub> sensors and have their own uncertainty of at least 20 % even after their correction.

## 3.5. Predicted and measured OA source contribution

In Thissio, during summer, the average measured total OA was 4.5  $\mu g \ m^{-3}$ , while the corresponding predicted concentration was 3  $\mu g \ m^{-3}$ . The PMF analysis of the OA AMS (Aerosol Mass Spectrometer) spectra indicated four factors: hydrocarbon-like OA (HOA), cooking OA (COA), low-oxygenated OA (LO-OOA) and more-oxygenated OA (MO-OOA). For our analysis, we have merged LO-OOA and MO-OOA into one factor,

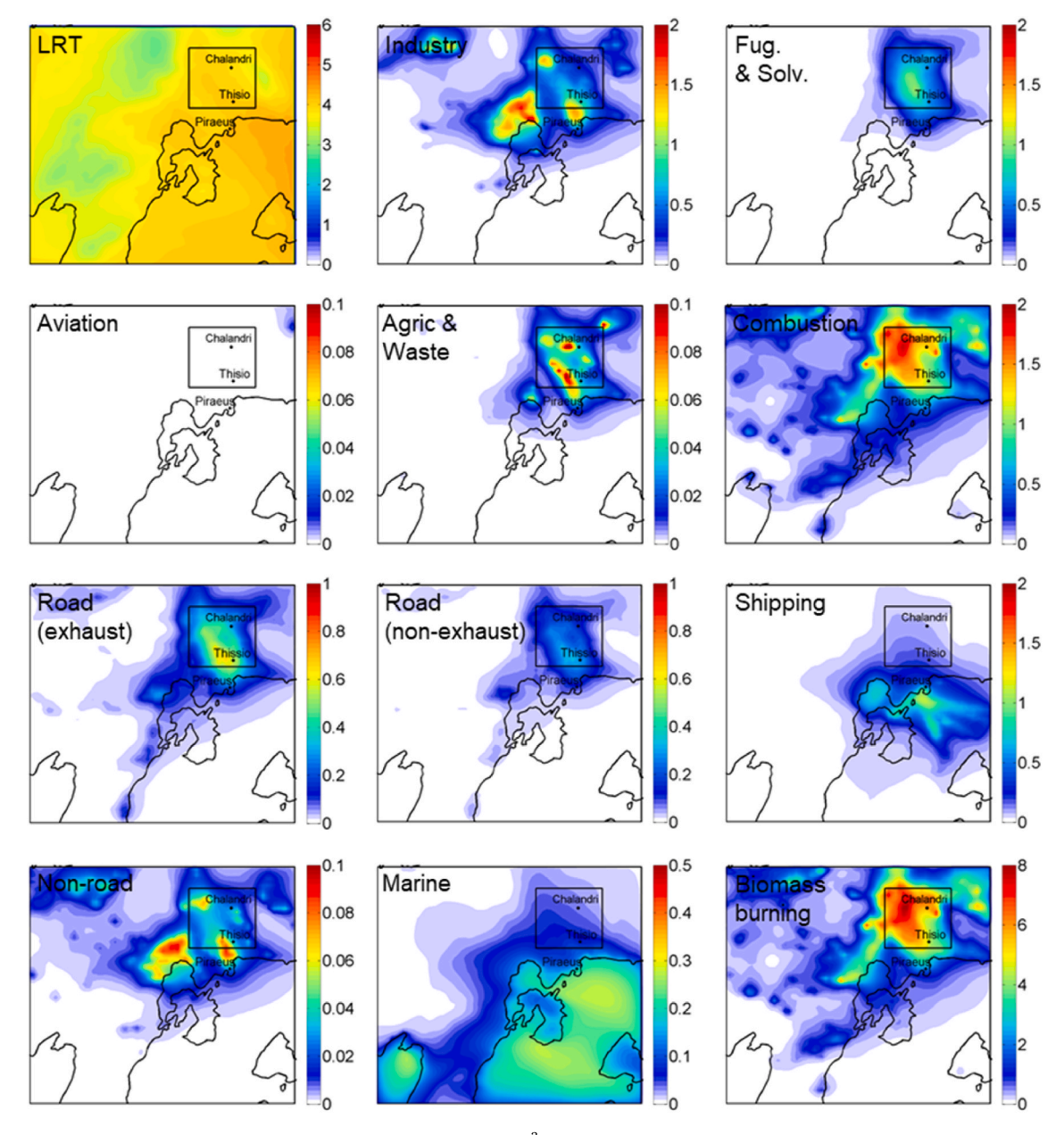


Fig. 5. Average predicted concentrations of  $PM_{2.5}$  from various sources in  $\mu g \ m^{-3}$  during January 2019 in Athens. Black boxes are used to represent Athens' urban center. Different scales are used.

the oxygenated OA (OOA) factor.

The average measured HOA concentration was  $0.34~\mu g~m^{-3}$ , while the predicted concentration was  $0.22~\mu g~m^{-3}$ . The sources of predicted HOA included all primary OA sources. For COA, the average measured concentration was equal to  $0.8~\mu g~m^{-3}$ , but COA emissions were not included in the current urban emission inventory. The average measured OOA concentration was  $3.5~\mu g~m^{-3}$ , whereas the average predicted one was  $2.8~\mu g~m^{-3}$ . The sources of predicted OOA included all secondary OA (biogenic and anthropogenic).

The model predictions can be used to provide insights about the sources of the factors resolved by the ACSM. PMCAMx predicted that 71 % of the total primary OA (HOA and BBOA for the AMS) originated from LRT (68 % wildfires and 3 % shipping), 13 % from local road transportation, 6 % from industry, and 4.5 % from combustion, with minor contributions from agriculture, shipping, and non-road transportation. For OOA in the same area, the model estimated that 95 % was due to sources outside the modeling domain. More specifically 44 % of the total OA was aged wildfire SOA, 15 % biogenic SOA, 5 % SOA from

agricultural waste burning, 4 % from fugitive emissions and solvents, 4 % from domestic combustion, 4 % from industry, 2 % from road transport, 1 % from non-road transport, 1 % from shipping and the remaining 15 % from sources outside Europe. These results suggest that the OOA is the result of the atmospheric chemical processing of the organic emissions of several sources, with biomass burning being the dominant one for Athens. The local SOA was 2 % from road transport with contributions below 1 % from several other local sources.

During the summer, the measured average diurnal profile of total OA is consistently higher than the predicted one, with a measured peak from 21:00 to 23:00 LT during the night, which was not predicted by PMCAMx (Fig. 8). These discrepancies are mainly related to underestimation of long-range transport of OA and to cooking emissions that were not included in the current emission inventory (Fig. S6).

During wintertime, ACSM measurements in Thissio suggested that the average measured concentration of total OA was 11  $\mu$ g m<sup>-3</sup>, while the corresponding predicted concentration was 9.5  $\mu$ g m<sup>-3</sup> for the period with available measurements (17–28/1). The PMF analysis for the

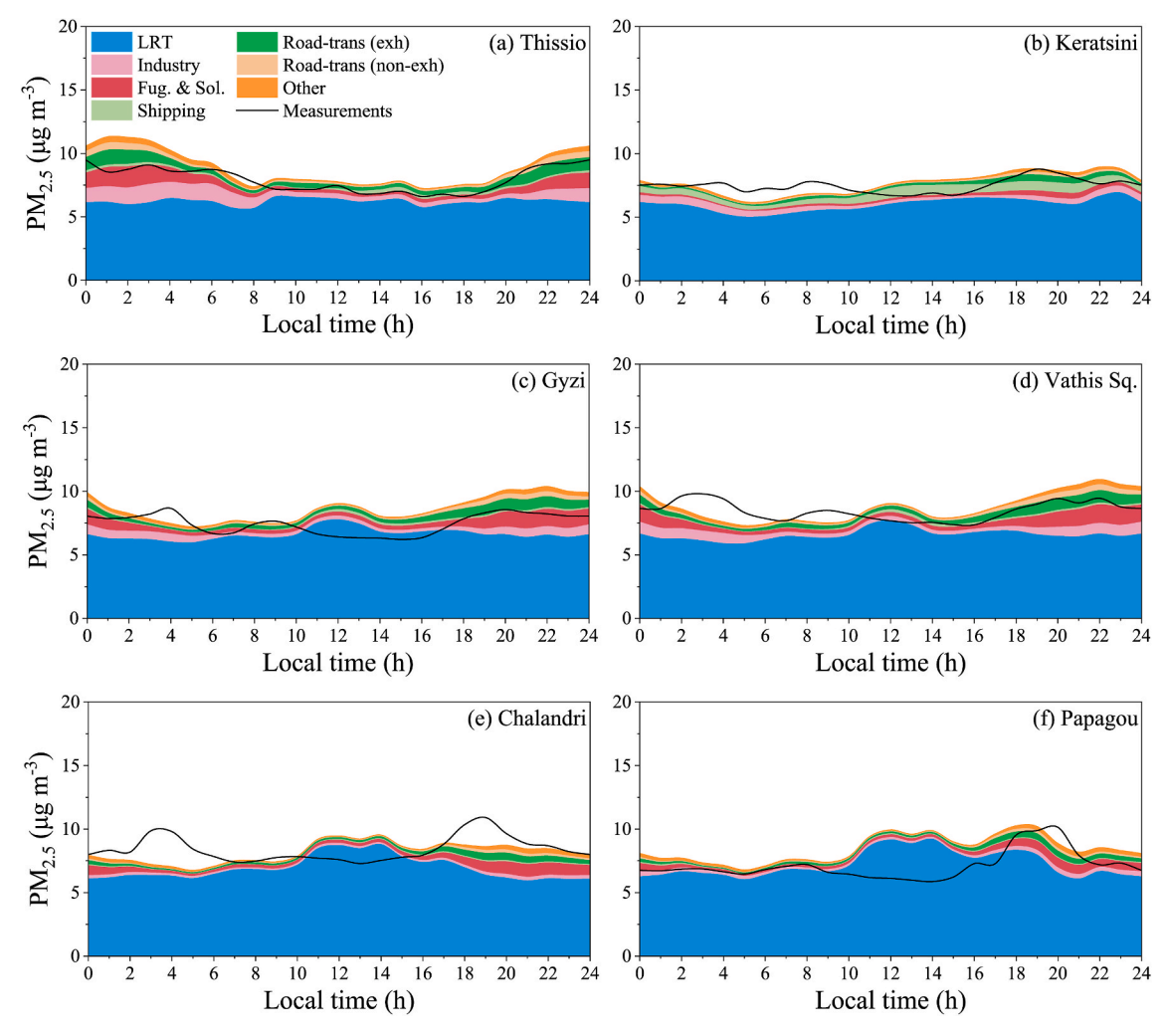


Fig. 6. Predicted average diurnal profiles for PM<sub>2.5</sub> sources and measured PM<sub>2.5</sub> for (a) Thissio, (b) Keratsini, (c) Gyzi, (d) Vathis Sq., (e) Chalandri and (f) Papagou during July 2019.

ambient OA indicated five factors for this period: hydrocarbon-like OA (HOA), cooking OA (COA), low-oxygenated OA (LO-OOA), more-oxygenated OA (MO-OOA) and biomass burning OA. The LO-OOA and MO-OOA factors were merged into one OOA factor.

The predicted and measured HOA average concentrations were equal to 1.1  $\mu g\ m^{-3}$ . According to the model 39 % of the predicted HOA was due to local domestic combustion (other than wood), 15 % to local road transportation, 5 % to shipping, 3 % to industrial sources, 3 % to nonroad transportation, and 2 % to local agriculture. The remaining 33 % of the predicted primary OA corresponding to HOA was due to sources outside Athens (75 % from marine and biogenic sources, 10 % from fugitives and solvents, 5 % from industry, and 4 % from aviation and the rest from other sources).

For COA, the average measured value was  $2 \, \mu g \, m^{-3}$ . This source was not included in the urban emission inventory as during summer and is responsible for most of the underprediction of total OA.

The average measured OOA concentration was 5.4  $\mu g$  m<sup>-3</sup>, whereas the corresponding predicted value was only 0.8  $\mu g$  m<sup>-3</sup>. Transport from outside the Athens area is predicted to be the main contributor to secondary OA during winter as the model predicted negligible local secondary OA production. The transported secondary OA was due to combustion (17 %), biogenic sources (8 %), fugitive emissions and solvents (3 %), road transport (3 %), industry (3 %), agricultural activities (3 %), shipping (2 %), wildfires (2 %) and road transport (1 %) with the remaining coming from sources outside Europe.

The average measured bbOA value was  $2.8 \,\mu g \, m^{-3}$ , almost half of the

predicted value of 6  $\mu g$  m $^{-3}$ . Practically all bbOA is predicted to be primary. Stavroulas et al. (2019) showed that LO-OOA and most of MO-OOA were due to biomass burning. The sum of measured OOA and bbOA (8.2  $\mu g$  m $^{-3}$ ) has a close value to the predicted value (6.8  $\mu g$  m $^{-3}$ ), but the model appears to miss an important pathway converting fresh bbOA to OOA during the winter nights.

The model reproduced the overall observed diurnal behavior of OA (Fig. 8). There was a peak during the nighttime, which was related to OOA based on measurements (Fig. S7). PMCAMx predicted also that this peak was due to residential biomass burning but that it was primary. OOA peaked during the night (Fig. S7), primarily due to the nighttime oxidation of bbOA based on Kodros et al. (2020), supporting the previous statement that the oxidized OA was attributed to bbOA by the model. PMCAMx lacks nighttime chemistry of bbOA and therefore it did not reproduce this peak.

#### 3.6. Average diurnal variability of EC

Elemental carbon model predictions were compared against available measurements in Thissio for the two periods (Fig. 9). During the summer, PMCAMx predicted that EC peaked during the night from 21:00 to 3:00 LT, mostly due to road transport. This behavior was not consistent with the measured values, which indicated a flat average EC diurnal profile. Also, there was a predicted peak in the morning related to road transport and another one at 3:00 LT due to EC transported from other areas. The difference is probably related to overestimations of the

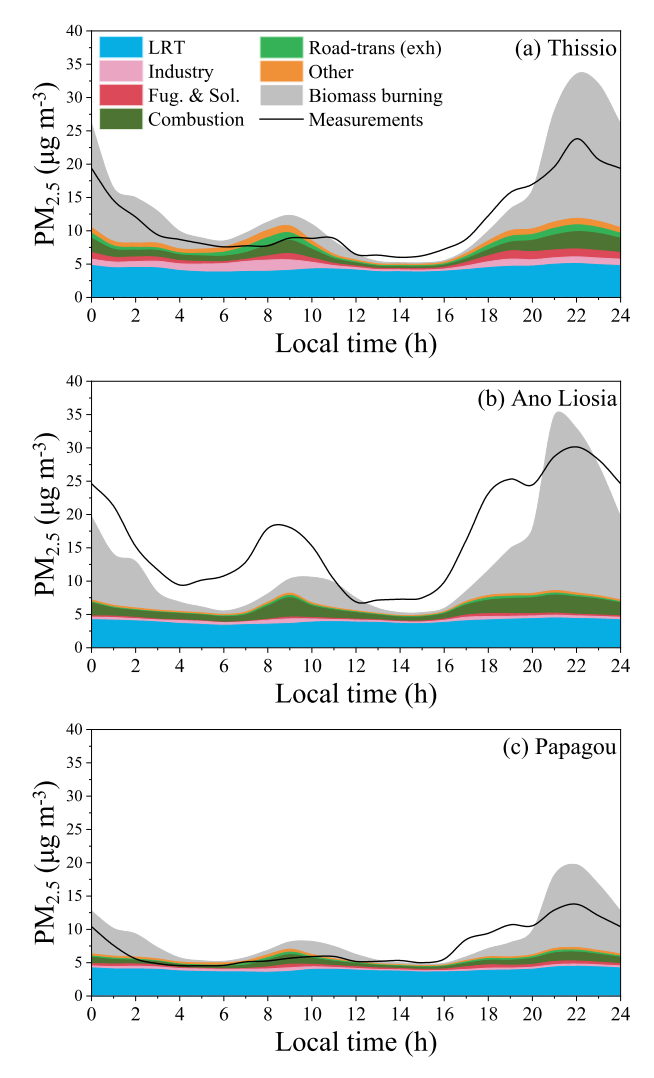


Fig. 7. Predicted average diurnal profiles for  $PM_{2.5}$  sources and measured  $PM_{2.5}$  for (a) Thissio, (b) Ano Liosia and (c) Papagou during January 2019.

#### corresponding emissions.

The average diurnal patterns of measured and predicted EC during the winter in Thissio were pretty similar. During the morning, at 9:00 LT, measurements showed a peak at 4  $\mu g$  m<sup>-3</sup>, which was also predicted by the model at the same time, but it was slightly underestimated. Based on PSAT, road transport and residential combustion were the major sources of EC during the morning. During the night, a peak of 4.5  $\mu$ g m<sup>-3</sup> was measured at 22:00 LT, which was also predicted by the model, but it was underestimated by 2  $\mu g$  m<sup>-3</sup>. PSAT predicted that residential combustion contributed 50 % of the EC during this period. The underestimation of the EC from residential heating was probably the major reason for the discrepancies in the peak values. During the rest of the day, both measurements and predictions were in satisfactory agreement. Discrepancies in the measurement methods for the emissions that are mostly EC and the ambient measurements that are BC can be a significant reason for the discrepancies between measurements and predictions.

#### 3.7. Source-resolved exposure to PM<sub>2.5</sub>

The population exposure histograms for the urban core for July and January 2019 are presented in Fig. 10. During summer, most people (60 %) were exposed on average to 8.2–9.2  $\mu g\ m^{-3}$  of PM<sub>2.5</sub>. All individuals were exposed to PM<sub>2.5</sub> levels above 5  $\mu g\ m^{-3}$ , but nobody was exposed to levels exceeding 10  $\mu g\ m^{-3}$ . A different population exposure profile was

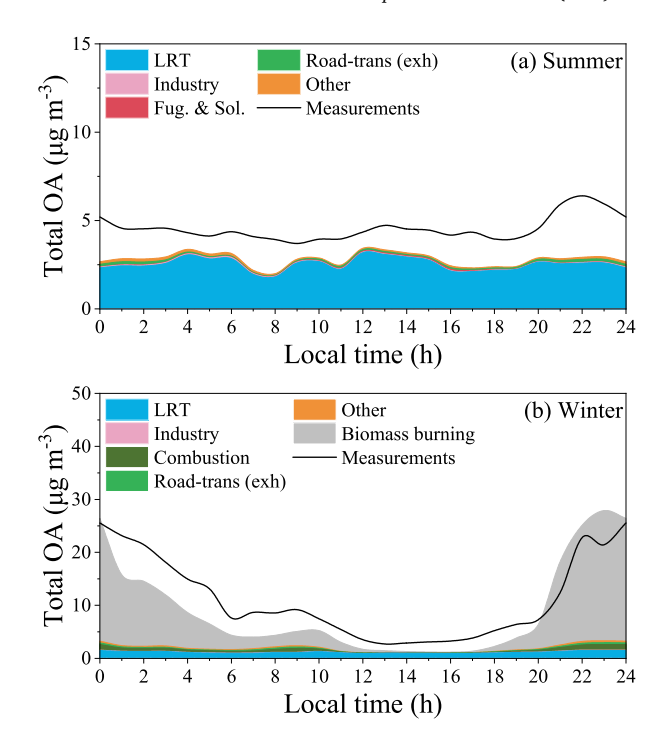
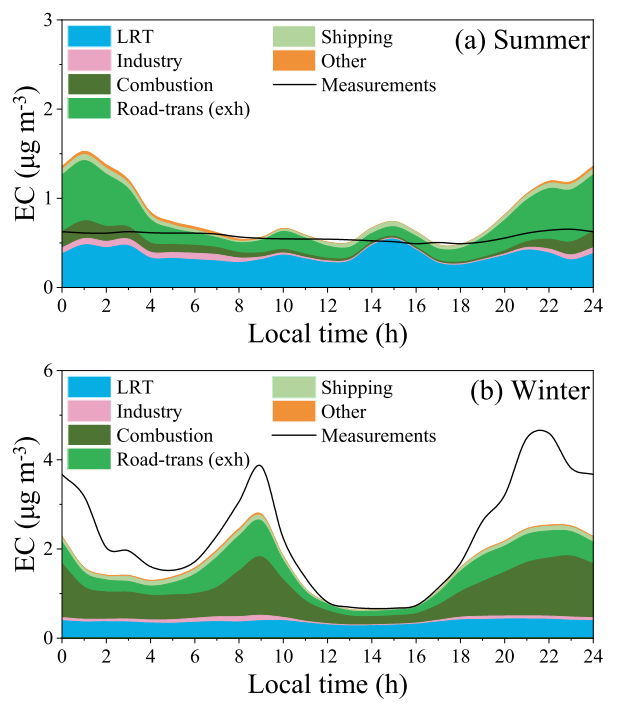


Fig. 8. Predicted and measured average diurnal profiles for OA and its predicted sources for Thissio during July and January 2019. Different scales are used.



**Fig. 9.** Predicted average diurnal profiles for EC sources and measured BC for Thissio during (a) July and (b) January 2019. Different scales are used.

predicted during the winter. In this case, people were exposed to a wider range of concentrations that varied from 3.2 to 16  $\mu g~m^{-3}.$  Approximately 60 % of the population was exposed to average  $PM_{2.5}$  concentrations above 10  $\mu g~m^{-3},$  while 98 % above 5  $\mu g~m^{-3}.$ 

Fig. 11 depicts the average predicted source contributions to  $PM_{2.5}$  mass concentrations and to  $PM_{2.5}$  exposure for the inner domain during summer and winter. The average predicted  $PM_{2.5}$  concentrations from

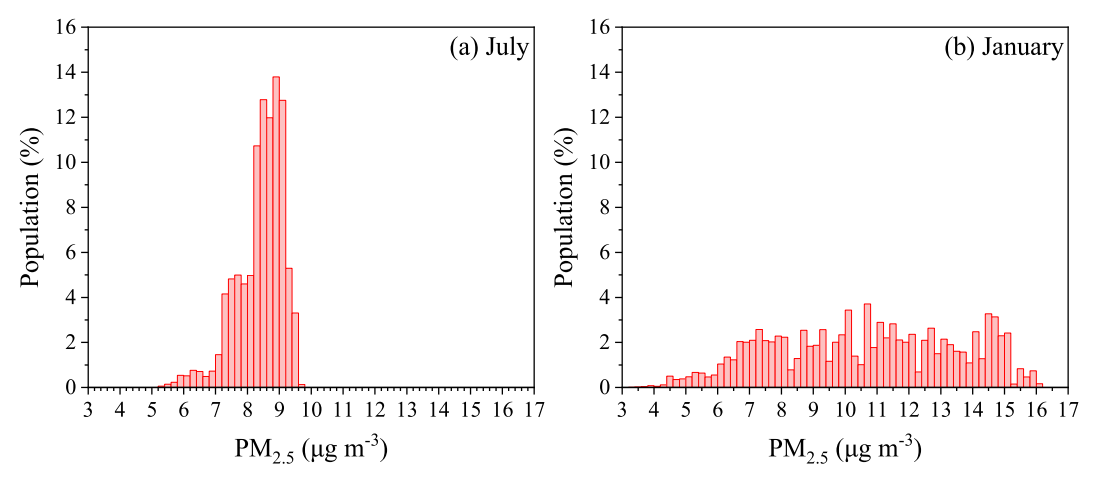


Fig. 10. Population PM<sub>2.5</sub> exposure distributions for the urban center during (a) July and (b) January 2019.

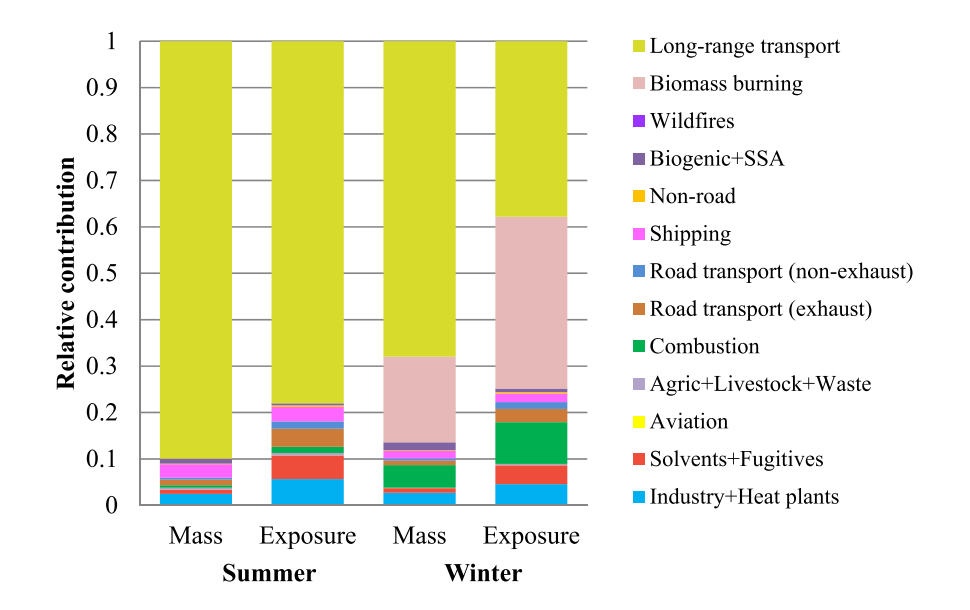


Fig. 11. Average relative source contributions to PM<sub>2.5</sub> mass and PM<sub>2.5</sub> exposure for the 1 × 1 km<sup>2</sup> modeling domain during July and January 2019.

each source are multiplied by the population distribution within the high-resolution domain to calculate the  $PM_{2.5}$  exposure. For the summer period, long-range transport was the dominant source of  $PM_{2.5}$  exposure (78 %) as for  $PM_{2.5}$  mass (90 %) (see also Fig. 2a). However, the local sources were twice as important for exposure as for the  $PM_{2.5}$  concentration. Transportation was the leading local source of  $PM_{2.5}$  exposure contributing 6 %, whereas shipping was the main local contributor to  $PM_{2.5}$  mass at 3 %. The main local sources of exposure, in descending order, were transportation (6 %), industry (5.5 %), fugitives and solvents (5 %), and shipping (3 %). Their spatial distributions are shown in Fig. S8. For  $PM_{2.5}$  mass, the primary local contributors were shipping (3 %), industry (2.5 %), transportation (1.6 %), and biogenic sources (1 %).

In winter, similar to summer, local sources were twice as significant for exposure as they were for concentration. For this period, local biomass burning accounted for 37 % of  $PM_{2.5}$  exposure, followed by combustion (9 %), transportation (6 %) and industry (6 %). Significant local contributions to  $PM_{2.5}$  mass were also residential biomass burning (19 %), combustion (5 %), industry (3 %) and transportation (1.6 %). Biomass burning was the most important local source of exposure in the urban core (Fig. S9).

#### 3.8. Effects of computational grid resolution

The low-resolution grid cannot reproduce the spatial concentration variations in urban sites. The 36  $\times$  36 km² resolution grid failed to capture the variability of PM<sub>2.5</sub> levels during summer (Fig. 12). PM<sub>2.5</sub> concentrations at the coarse grid level were relatively uniform, ranging from 5 to 6.4  $\mu g$  m $^{-3}$  across the entire modeling domain. The average peak PM<sub>2.5</sub> increased by 35 % moving from the coarse (36  $\times$  36 km²) to the fine grid resolution (1  $\times$  1 km²). For OA, the peak level increased by 63 % and for the EC by 80 % in the fine scale.

During wintertime, the effects of the grid resolution were even more pronounced (Fig. 13). The corresponding increases of predicted maximum levels were 64 % for PM $_{2.5}$ , 88 % for OA, and almost a factor of two for EC. The main reason for the significant spatial variability in PM $_{2.5}$  and OA during winter was the local source of residential biomass burning. The use of nesting ending up in the fine resolution of  $1\times 1~{\rm km}^2$  appears to be necessary for accurately resolving PM $_{2.5}$  high-concentration areas during the winter, more so than in the summer.

#### 4. Conclusions

The widely used PSAT source-apportionment algorithm was

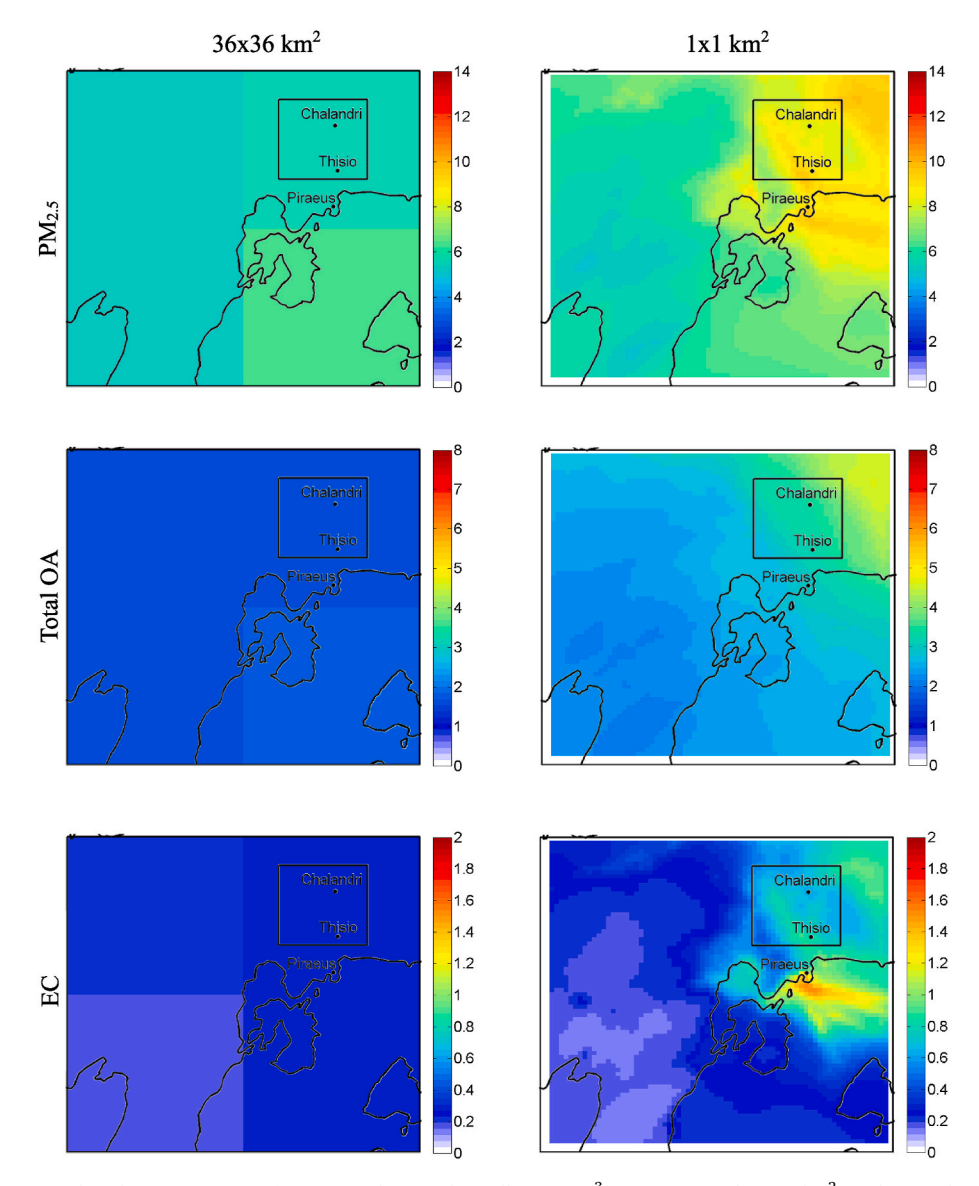


Fig. 12. Average predicted concentrations of PM<sub>2.5</sub>, total OA and EC all in  $\mu g \ m^{-3}$  at 36  $\times$  36 and 1  $\times$  1 km<sup>2</sup> resolutions during July 2019.

enhanced in this study to calculate source contributions across multiple grids, moving from regional to urban scales with progressively higher spatial resolution up to 1  $\times$  1 km². We applied our approach to the concentrations and sources of PM $_{2.5}$ , OA, and EC in Athens during a typical summer and winter month.

In summer, long-range transport was the main source of  $PM_{2.5}$ , OA, and EC, even at the sites with the highest concentrations, with local sources making smaller contributions. In winter, while long-range transport remained a significant source of  $PM_{2.5}$ , residential biomass burning was the predominant local source contributing 37 % in the urban core. Small  $PM_{2.5}$  concentration gradients were predicted in summer, consistent with the available observations. However, in winter, sharp concentration gradients were present in the urban core, with average  $PM_{2.5}$  concentrations doubling within 5 km due to residential biomass burning. Also, during the winter nights, both measurements and predictions indicated high hourly  $PM_{2.5}$  levels due to intense local residential biomass burning.

There was a tendency towards underprediction of the low summertime OA levels probably due to an underestimation of OA contributions from long-range transport. At night, the underpredicted OA peak was primarily attributed to the absence of cooking emissions in the current emission inventory. In winter, the model effectively captured the overall

trend of observed OA in the urban center, with good agreement between predicted and observed values. However, the lack of nighttime oxidation of bbOA led the model to associate high OA peaks with primary sources rather than secondary ones.

Long-range transport dominated  $PM_{2.5}$  mass and exposure, while local sources like transportation contributed more to exposure than mass. In winter, local sources, particularly biomass burning, became more significant, especially for exposure. The findings underscore the importance of high-resolution grids in accurately capturing spatial variability in  $PM_{2.5}$ , OA, and EC concentrations, particularly in urban areas where local sources like residential biomass burning play a critical role. The substantial increases in spatial variability observed at finer resolutions, especially during winter, highlight the limitations of coarse grids in resolving localized pollution hotspots.

Differences between measured and predicted values arise for several reasons. One major factor is the underestimation of emissions from cooking during the summer, which contributed significantly to the discrepancies between predicted and observed OA levels. Additionally, the absence of nighttime chemistry in the model resulted in further differences, particularly due to the nighttime oxidation of bbOA, which PMCAMx failed to predict. Regarding emissions, a more detailed inventory and a re-estimation of residential biomass burning emissions are

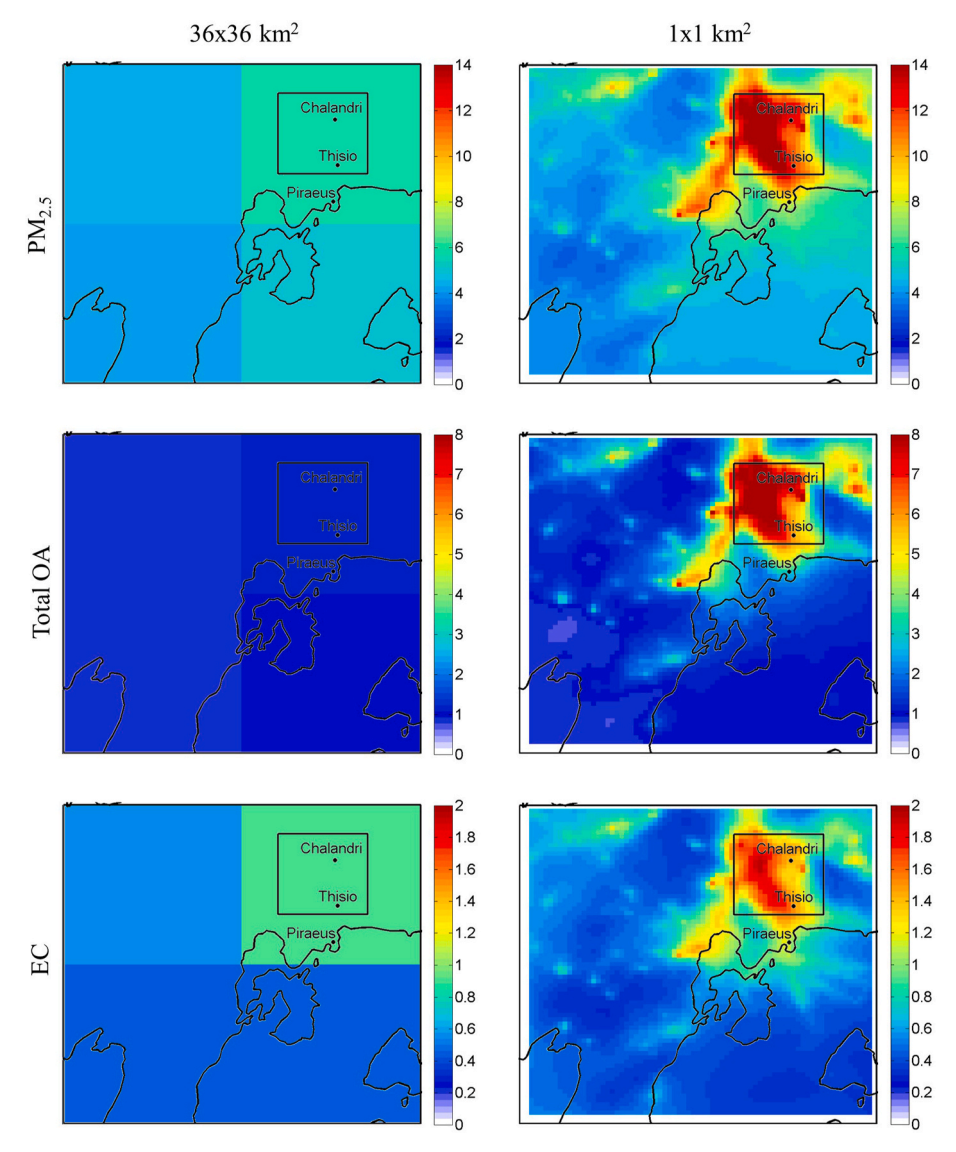


Fig. 13. Average predicted concentrations of PM<sub>2.5</sub>, total OA and EC all in  $\mu g \ m^{-3}$  at 36  $\times$  36 and 1  $\times$  1 km<sup>2</sup> resolutions during January 2019.

necessary to better represent winter pollution. Uncertainty also arises from the use of low-cost sensors in the measurement network and the meteorological data.

The results of this analysis provide valuable information about the sources responsible for the exposure of the residents of Athens to fine particulate matter. Most of these sources are located outside Athens with wildfires dominating during the summer. Local biomass burning during the winter deserves immediate regulatory attention. Other combustion sources during the winter and shipping emissions are the next most important local sources. Road transportation that receives most of the regulatory attention is predicted to be a minor source of PM<sub>2.5</sub>.

## CRediT authorship contribution statement

Evangelia Siouti: Writing – review & editing, Writing – original draft, Software, Methodology, Investigation, Formal analysis, Conceptualization. Ksakousti Skyllakou: Writing – review & editing, Software, Investigation. David Patoulias: Writing – review & editing, Software, Formal analysis, Data curation. Eleni Athanasopoulou: Writing – review & editing, Investigation, Data curation. Nikolaos Mihalopoulos: Writing – review & editing, Supervision. Jeroen Kuenen: Writing – review & editing, Methodology, Data curation. Spyros N. Pandis: Writing – review & editing, Supervision, Methodology,

Conceptualization.

## **Declaration of competing interest**

The authors declare that they have no known competing financial interests or personal relationships that could have appeared to influence the work reported in this paper.

#### Acknowledgements

This work was supported by the EU H2020 Research Infrastructures Services Reinforcing Air Quality Monitoring Capacities in European Urban & Industrial AreaS (RI-URBANS) project (grant 101036245) and the project NANOSOMs Grant 11504 of the Greek HFRI.

## Appendix A. Supplementary data

Supplementary data to this article can be found online at  $\frac{https:}{doi.}$  org/10.1016/j.atmosenv.2025.121277.

## Data availability

Data will be made available on request.

#### References

- Capaldo, K.P., Pilinis, C., Pandis, S.N., 2000. A computationally efficient hybrid approach for dynamic gas/aerosol transfer in air quality models. Atmos. Environ. 34, 2617, 2627.
- Carter, W.P.L., 2000. Documentation of the SAPRC-99 chemical mechanism for VOC reactivity assessment. Report to California air resources board. https://intra.engr.ucr.edu/~carter/absts.htm#saprc99.
- Coelho, S., Ferreira, J., Rodrigues, V., Lopes, M., 2022. Source apportionment of air pollution in European urban areas: lessons from the ClairCity project. JEM (J. Emerg. Med.) 320, 115899.
- Deng, Q., Deng, L., Miao, Y., Guo, X., Li, Y., 2019. Particle deposition in the human lung: health implications of particulate matter from different sources. Environ. Res. 169, 237–245. https://doi.org/10.1016/j.envres.2018.11.014.
- Diapouli, E., Manousakas, M., Vratolis, S., Vasilatou, V., Maggos, T., Saraga, D., Grigoratos, Th, Argyropoulos, G., Voutsa, D., Samara, C., Eleftheriadis, K., 2017. Evolution of air pollution source contributions over one decade, derived by PM<sub>10</sub> and PM<sub>2.5</sub> source apportionment in two metropolitan urban areas in Greece. Atmos. Environ. 164. 416–430.
- Dimitriou, K., Stavroulas, I., Grivas, G., Chatzidiakos, C., Kosmopoulos, G., Kazantzidis, A., Kourtidis, K., Karagioras, A., Hatzianastassiou, N., Pandis, S.N., Mihalopoulos, N., Gerasopoulos, E., 2023. Intra- and inter-city variability of PM<sub>2.5</sub> concentrations in Greece as determined with a low-cost sensor network. Atmos. Environ. 301, 119713.
- Donahue, N.M., Robinson, A.L., Stanier, C.O., Pandis, S.N., 2006. Coupled partitioning, dilution, and chemical aging of semivolatile organics. Environ. Sci. Technol. 40, 2635–2643. https://doi.org/10.1021/es052297c.
- Environmental Protection Agency (EPA), 2023. Health and environmental effects of particulate matter (PM). https://www.epa.gov/pm-pollution/health-and-environmental-effects-particulate-matter-pm.
- European Environmental Agency (EEA), 2023. Premature deaths due to exposure to fine particulate matter in Europe. https://www.eea.europa.eu/en/analysis/indicators/health-impacts-of-exposure-to.
- Fahey, K.M., Pandis, S.N., 2001. Optimizing model performance: variable size resolution in cloud chemistry modeling. Atmos. Environ. 35, 4471–4478. https://doi.org/ 10.1016/S1352-2310(01)00224-2.
- Fann, N., Lamson, A.D., Anenberg, S.C., Wesson, K., Risley, D., Hubbell, B.J., 2012. Estimating the national public health burden associated with exposure to ambient PM<sub>2.5</sub> and ozone. Risk Anal. 32, 81–95. https://doi.org/10.1111/j.1539-6924.2011.01630.x.
- Feng, S., Gao, D., Liao, F., Zhou, F., Wang, X., 2016. The health effects of ambient PM<sub>2.5</sub> and potential mechanisms. Ecotoxicol. Environ. Saf. 128, 67–74. https://doi.org/10.1016/j.ecoenv.2016.01.030.
- Fountoukis, C., Racherla, P.N., Denier Van Der Gon, H.A.C., Polymeneas, P., Charalampidis, P.E., Pilinis, C., Wiedensohler, A., Dall'Osto, M., O'Dowd, C., Pandis, S.N., 2011. Evaluation of a three-dimensional chemical transport model (PMCAMx) in the European domain during the EUCAARI May 2008 campaign. Atmos. Chem. Phys. 11, 10331–10347.
- Garcia Rivera, P., Dinkelacker, B.T., Kioutsioukis, I., Adams, P.J., Pandis, S.N., 2022. Source-resolved variability of fine particulate matter and human exposure in an urban area. Atmos. Chem. Phys. 22, 2011–2027. https://doi.org/10.5194/acp-22-2011-2022.
- Grivas, G., Cheristanidis, S., Chaloulakou, A., Koutrakis, P., Mihalopoulos, N., 2018. Elemental composition and source apportionment of fine and coarse particles at traffic and urban background locations in Athens, Greece. AAQR 18, 1642–1659. https://doi.org/10.4209/aaqr.2017.12.0567.
- Huang, F., Pan, B., Wu, J., Chen, E., Chen, L., 2017. Relationship between exposure to PM<sub>2.5</sub> and lung cancer incidence and mortality: a meta-analysis. Oncotarget 8, 43322–43331. https://doi.org/10.18632/oncotarget.17313.
- Kodros, J.K., Papanastasiou, D.K., Paglione, M., Masiol, M., Squizzato, S., Florou, K., Skyllakou, K., Kaltsonoudis, C., Nenes, A., Pandis, S.N., 2020. Rapid dark aging of biomass burning as an overlooked source of oxidized organic aerosol. Proc. Natl. Acad. Sci. USA. 117 (52), 33028–33033. https://doi.org/10.1073/pnss.2010365117
- Kosmopoulos, G., Salamalikis, V., Pandis, S.N., Yannopoulos, P., Bloutsos, A.A., Kazantzidis, A., 2020. Low-cost sensors for measuring airborne particulate matter: field evaluation and calibration at a South-Eastern European site. Sci. Total Environ. 748, 141396. https://doi.org/10.1016/j.scitotenv.2020.141396.
- Kuenen, J., Dellaert, S., Visschedijk, A., Jalkanen, J.P., Super, I., Denier van der Gon, H., 2022. CAMS-REG-v4: a state-of-the-art high-resolution European emission inventory for air quality modelling. Earth Syst. Sci. Data 14, 491–515.
- Morris, R.E., Mc Nally, D.E., Tesche, T.W., Tonnesen, G., Boylan, J.W., Brewer, P., 2005. Preliminary evaluation of the community multiscale air quality model for 2002 over the southeastern United States. J. Air Waste Manag. Assoc. 55, 1694–1708. https://doi.org/10.1080/10473289.2005.10464765.
- Pateraki, S., Asimakopoulos, D.N., Maggos, T., Assimakopoulos, V.D., Bougiatioti, A., Bairachtari, K., Vasilakos, C., Mihalopoulos, N., 2020. Chemical characterization, sources and potential health risk of PM<sub>2.5</sub> and PM<sub>1</sub> pollution across the Greater Athens Area. Chemosphere 241, 125026. https://doi.org/10.1016/j.chemosphere.2019.125026.

- Pepe, N., Pirovano, G., Balzarini, A., Toppetti, A., Riva, G.M., Amato, F., Lonati, G., 2019. Enhanced CAMx source apportionment analysis at an urban receptor in Milan based on source categories and emission regions. Atmos. Environ. X 2, 100020. https://doi. org/10.1016/j.aeaoa.2019.100020.
- Ramacher, M.O.P., Kakouri, A., Speyer, O., Feldner, J., Karl, M., Timmermans, R., Denier van der Gon, H., Kuenen, J., Gerasopoulos, E., Athanasopoulou, E., 2021. The UrbEm hybrid method to derive high-resolution emissions for city-scale air quality modeling. Atmosphere 12, 1404. https://doi.org/10.3390/atmos12111404.
- Saraga, D., Maggos, T., Degrendele, C., Klanova, J., Horvat, M., Kocman, D., Kanduc, T., Dos Santos, S.G., Franco, R., Gomez, P.M., Manousakas, M., Bairachtari, K., Eleftheriadis, K., Kermenidou, M., Karakitsios, S., Gotti, A., Sarigiannis, D., 2021. Multi-city comparative PM<sub>2.5</sub> source apportionment for fifteen sites in Europe: the ICARUS project. Sci. Total Environ. 751, 141855
- Seinfeld, J.H., Pandis, S.N., 2006. Atmospheric Chemistry and Physics: from Air Pollution to Climate Change. John Wiley and Sons, Hoboken, New Jersey.
- Siouti, E., Skyllakou, K., Kioutsioukis, I., Patoulias, D., Apostolopoulos, I.D., Fouskas, G., Pandis, S.N., 2024. Prediction of the concentration and source contributions of PM<sub>2.5</sub> and gas-phase pollutants in an urban area with the SmartAQ forecasting system. Atmosphere 15, 8. https://doi.org/10.3390/atmos15010008.
- Siouti, E., Skyllakou, K., Kioutsioukis, I., Patoulias, D., Fouskas, G., Pandis, S.N., 2022. Development and application of the SmartAQ high-resolution air quality and source apportionment forecasting system for European urban areas. Atmosphere 13, 1–20. https://doi.org/10.3390/atmosl3101693.
- Skamarock, W.C., Klemp, J.B., Dudhia, J., Gill, D.O., Liu, Z., Berner, J., Wang, W., Powers, J.G., Duda, M.G., Barker, D.M., 2019. A Description of the Advanced Research WRF Model Version 4.1. https://doi.org/10.5065/1dfh-6p97 (No. NCAR/TN-556+STR).
- Skyllakou, K., Murphy, B.N., Megaritis, A.G., Fountoukis, C., Pandis, S.N., 2014. Contributions of local and regional sources to fine PM in the megacity of Paris. Atmos. Chem. Phys. 14, 2343–2352.
- Skyllakou, K., Rivera, P.G., Dinkelacker, B., Karnezi, E., Kioutsioukis, I., Hernandez, C., Adams, P.J., Pandis, S.N., 2021. Changes in PM<sub>2.5</sub> concentrations and their sources in the US from 1990 to 2010. Atmos. Chem. Phys. 21, 17115–17132.
- Skyllakou, K., Fountoukis, C., Charalampidis, P., Pandis, S.N., 2017. Volatility-resolved source apportionment of primary and secondary organic aerosol over Europe. Atmos. Environ. 167, 1–10.
- Slinn, S.A., Slinn, W.G.N., 1980. Predictions for particle deposition on natural waters. Atmos. Environ. 14, 1013–1016. https://doi.org/10.1016/0004-6981(80)90032-3.
- Stavroulas, I., Bougiatioti, A., Grivas, G., Paraskevopoulou, D., Tsagkaraki, M., Zarmpas, P., Liakakou, E., Gerasopoulos, E., Mihalopoulos, N., 2019. Sources and processes that control the submicron organic aerosol composition in an urban Mediterranean environment (Athens): a high temporal-resolution chemical composition measurement study. Atmos. Chem. Phys. 19 (2), 901–919. https://doi.org/10.5194/acp.19-901-2019.
- Tambour, Y., Seinfeld, J.H., 1980. Solution of the discrete coagulation equation.
  J. Colloid Interface Sci. 74, 260–272. https://doi.org/10.1016/0021-9797(80)
  90189-7.
- Theodosi, C., Tsagkaraki, M., Zarmpas, P., Liakakou, E., Grivas, G., Paraskevopoulou, D., Lianou, M., Gerasopoulos, E., Mihalopoulos, N., 2018. Multi-year chemical composition of the fine-aerosol fraction in Athens, Greece, with emphasis on the contribution of residential heating in wintertime. Atmos. Chem. Phys. 18 (19), 14371–14391.
- Thunis, P., Degraeuwe, B., Pisoni, E., Trombetti, M., Peduzzi, E., Belis, C.A., Wilson, J., Clappier, A., Vignati, E., 2018. PM<sub>2.5</sub> source allocation in European cities: a SHERPA modelling study. Atmos. Environ. 187, 93–106.
- Tsimpidi, A.P., Karydis, V.A., Zavala, M., Lei, W., Molina, L., Ulbrich, I.M., Jimenez, J.L., Pandis, S.N., 2010. Evaluation of the volatility basis-set approach for the simulation of organic aerosol formation in the Mexico City metropolitan area. Atmos. Chem. Phys. 10, 525–546.
- Wagstrom, K.M., Pandis, S.N., 2011a. Source receptor relationships for fine particulate matter concentrations in the Eastern United States. Atmos. Environ. 45, 347–356.
- Wagstrom, K.M., Pandis, S.N., 2011b. Contribution of long-range transport to local fine particulate matter concerns. Atmos. Environ. 45, 2730–2735.
- Wagstrom, K.M., Pandis, S.N., Yarwood, G., Wilson, G.M., Morris, R.E., 2008.
  Development and application of a computationally efficient particulate matter apportionment algorithm in a three-dimensional chemical transport model. Atmos. Environ. 42, 5650–5659.
- Wesely, M.L., 2007. Parameterization of surface resistances to gaseous dry deposition in regional-scale numerical models. Atmos. Environ. 41, 52–63. https://doi.org/ 10.1016/j.atmosenv.2007.10.058.
- Zhang, Q., Jimenez, J.L., Canagaratna, M.R., Allan, J.D., Coe, H., Ulbrich, I., Alfarra, M. R., Takami, A., Middlebrook, A.M., Sun, Y.L., Dzepina, K., Dunlea, E., Docherty, K., De-Carlo, P.F., Salcedo, D., Onasch, T., Jayne, J.T., Miyoshi, T., Shimono, A., Hatakeyama, S., Takegawa, N., Kondo, Y., Schneider, J., Drewnick, F., Borrmann, S., Weimer, S., Demerjian, K., Williams, P., Bower, K., Bahreini, R., Cottrell, L., Griffin, R.J., Rautiainen, J., Sun, J.Y., Zhang, Y.M., Worsnop, D.R., 2007. Ubiquity and dominance of oxygenated species in organic aerosols in anthropogenically-influenced northern hemisphere midlatitudes. Geophys. Res. Lett. 34, L13801. https://doi.org/10.1029/2007gl029979.